Journal of Materials Chemistry A

PAPER

View Article Online
View Journal | View Issue

Cite this: J. Mater. Chem. A, 2018, 6, 14315

A novel epoxy resin-based cathode binder for low cost, long cycling life, and high-energy lithium–sulfur batteries†

Longlong Yan,‡[ab] Xiguang Gao,‡[b] Farihah Wahid-Pedro,[b] Jesse Thomas Ernest Quinn,[b] Yuezhong Meng *[a] and Yuning Li *[b]

Received 13th May 2018
Accepted 28th June 2018

DOI: 10.1039/c8ta04450c

rsc.li/materials-a

An epoxy resin PEI–ER formed by *in situ* cross-linking between an epoxide compound (ER) and polyethylenimine (PEI) is developed as a new cathode binder for lithium–sulfur (Li–S) batteries. Li–S batteries using this new binder showed high initial specific capacity along with remarkable cycling stability. A composite interlayer of PEI–ER and carbon black is also developed to further enhance the cycling stability. A Li–S battery using a combination of the new binder and interlayer achieved a high initial specific capacity of 1174 mA h g^{-1} and an excellent capacity retention of 80% after 1000 cycles at a cycling rate of 0.5C with 70 wt% sulfur content in the cathode and an areal sulfur loading of 1.9 mg cm^{-2}, which is among the best cycling stabilities reported for Li–S batteries to date. A Li–S battery with a high areal sulfur loading of 5.4 mg cm^{-2} demonstrated an initial capacity of 780 mA h g^{-1}, which corresponds to a high areal capacity of 4.2 mA h cm^{-2}, and an excellent capacity retention of 72% after 500 cycles.

Introduction

With a high theoretical specific energy of ~2600 W h kg^{-1} and abundant sulfur sources in nature, lithium–sulfur (Li–S) batteries have been considered to be one of the most promising high energy density and low-cost rechargeable battery technologies for electric vehicles (EVs), hybrid electric vehicles (HEVs) and portable devices.[1–4] Despite decades of research and development, the performance of Li–S batteries still leaves much to be desired, particularly in terms of energy density (or specific capacity of the sulfur cathode) and cycling stability. The issues mainly originate from (i) the extremely low electrical conductivity of sulfur (5×10^{-30} S cm^{-1}) that results in an ineffective use of sulfur, (ii) the large volume change (up to 76%) between elemental sulfur in the charged state and lithium sulfides in the discharged state during battery cycling, which causes a severe damage to the cathode structure, and (iii) migration of the soluble intermediate polysulfides (Li_2S_x, where x = 3–8) towards the Li anode during discharging and their shuttling back to the cathode during charging, which reduce the sulfur utilization.[5–11] To improve the specific capacity of the sulfur cathode, the use of a highly conductive material to blend with sulfur and a reduction of the sulfur particle size into the nanometer regime, which can assist charge transport between sulfur and the electrode, have proven to be effective.[12] In comparison to the specific capacity, it appears to be more challenging to improve the cycling stability of the cathode material. Among many approaches of encapsulating sulfur, incorporation of host nanostructured materials such as porous carbon, carbon nanotubes, and graphene[13–16] has been proven to be the best approach so far.[17] These efforts have significantly improved the Li–S battery cycling time from tens of cycles in 2009 (ref. 13) to up to hundreds of cycles nowadays.[17] To prevent the dissolution and diffusion of polysulfides, additives that can strongly interact or form chemical bonds with polysulfides such as metal oxides[18] and N (nitrogen)-doped carbon materials[19–21] were found to be effective.

Nonetheless, the majority of approaches adopted so far have been focused on the improvement of either the specific capacity or cycling life of the Li–S batteries separately.[17] Li–S batteries with both high capacity and long cycling life are rarely reported. Furthermore, many reported high performance Li-batteries used very expensive additives and elaborate processes to fabricate the sulfur cathode, which will be barriers to commercialization.

In order to meet the high energy density requirement, a minimum sulfur content of 70 wt% in the cathode is needed.[22]

[a]The Key Laboratory of Low-Carbon Chemistry & Energy Conservation of Guangdong Province, State Key Laboratory of Optoelectronic Materials and Technologies, School of Materials Science and Engineering, Sun Yat-sen University, Guangzhou 510275, P. R. China. E-mail: mengyzh@sysu.edu.cn

[b]Department of Chemical Engineering, Waterloo Institute for Nanotechnology (WIN), University of Waterloo, 200 University Ave West, Waterloo, Ontario, Canada, N2L 3G1. E-mail: yuning.li@uwaterloo.ca; Fax: +1-519-888-4347; Tel: +1-519-888-4567 ext. 31105

† Electronic supplementary information (ESI) available. See DOI: 10.1039/c8ta04450c

‡ These authors contributed equally to this work.

The sulfur cathode in a typical Li–S battery is comprised of 70 wt% sulfur, 20 wt% conductive component, and 10 wt% polymer binder. The polymer binder holds sulfur and the conductive component (*e.g.* carbon black) together and maintains strong adhesion of the active materials to the current collector. Polyvinylidene fluoride (PVDF) is the most widely used binder for Li–S batteries. However, at such a low loading amount (~10 wt%), the polymer network formed by the entanglement of PVDF polymer chains through interchain van der Waals forces is expected to be weak and fails to maintain the structural integrity of the cathode material after repeated charge/discharge cycling. Some previous studies show that the cycling stability and capacity of Li–S batteries could be notably improved by using some alternative binders to PVDF.[23–31] In this study, we developed a novel polymer binder based on a cross-linked epoxy resin, which can be readily prepared *in situ* to form a robust network structure *via* strong covalent bonds to confine sulfur and the conductive component in the cathode. Very high specific capacity and excellent cycling stability have been achieved by using this cathode binder for Li–S batteries.

Results and discussion

Epoxy resins have been widely used for many years in paints, coatings, adhesives, engineering plastics, *etc.* for a large variety of industrial and consumer applications because of their superb mechanical properties, ease of processing, and low cost. In this study, an oligomeric bisphenol A diglycidyl ether (ER), and a polyamine hardener, a highly branched polyethylenimine (PEI), are chosen. The step-growth polymerization of ER and PEI to form a cross-linked network (PEI–ER) (Fig. 1a) involves the reactions of epoxide (or glycidyl) groups of ER with the primary ($-NH_2$) and secondary (–NH–) amine groups of PEI and the hydroxyl (–OH) groups of the intermediate products formed through ring-opening of the epoxide groups. The choice of this epoxy resin composition as a binder is based on several considerations. First, these two compounds are commercially readily available and inexpensive. Second, previous computational simulation studies have shown that nitrogen and oxygen atoms have strong binding energies to lithium polysulfides by forming a coordination bond between nitrogen or oxygen and lithium atoms.[32] The NH_2, –NH–, and –OH groups may also form a hydrogen bond with lithium polysulfides.[33,34] Third, the highly branched structure of PEI would form a highly cross-linked 3-D network structure for a stronger confinement of sulfur and the conductive component and to buffer the volume change between the elemental sulfur and sulfides during the discharge/charge process.

To verify the sulfide binding effects of nitrogen and oxygen atoms in PEI and ER, the adsorption binding energies (E_d) of the PEI–ER binder to lithium sulfides (Li_2S_x) with up to 8 sulfur atoms (x = 1–4, 6, and 8) were calculated by using density functional theory (DFT). Representative polymer segments of PEI, ER, or the reference PVDF (Fig. 1b and S1–S5†) are used for the calculations, where two neighboring N atoms, O atoms, or F atoms are assumed to interact with one Li ion of a Li_2S_x. The results clearly revealed that the E_ds with Li_2S_x are in the order of

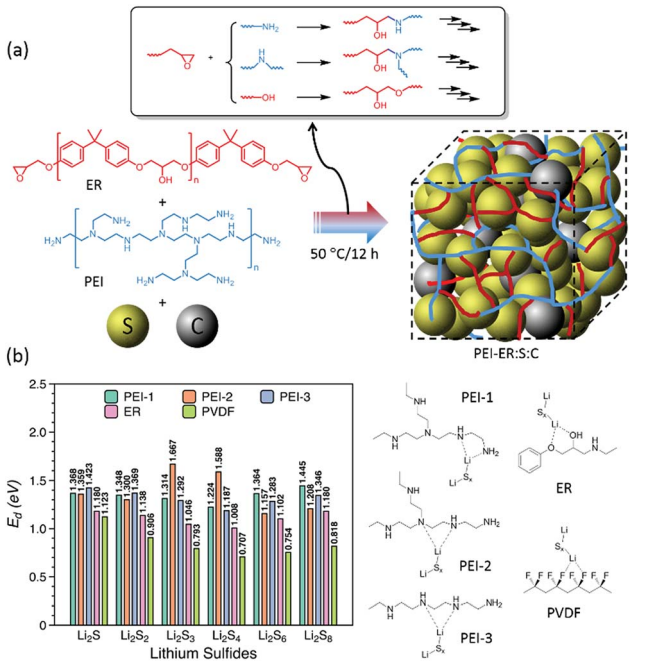

Fig. 1 (a) *In situ* step-growth polymerization of polyethylenimine (PEI) and epoxy resin (ER) in the presence of sulfur (S) and conductive carbon black (C) to form a PEI–ER:S:C cathode composite material, where S and C particles are tightly held by the highly cross-linked 3-D PEI–ER network. (b) The adsorption binding energies (E_d's) of the representative nitrogen atoms in PEI, oxygen atoms in ER, and fluorine atoms in PDVF with some lithium sulfides. Note that the abnormally high E_d obtained between PEI-2 and Li_2S_3 or Li_2S_4 is due to the additional interaction of a third neighboring nitrogen atom (see Fig. S2†).

PEI > ER > PVDF for all the sulfide species calculated (Fig. 1b). Especially, the E_ds of PEI and ER towards longer sulfides (x > 2) are significantly greater than the corresponding E_ds of PVDF. It is interesting to note that when Li_2S_3 or Li_2S_4 was set to interact with one secondary N atom and one tertiary N atom in PEI-2, another neighboring secondary N atom was also found to bind with the same Li ion, forming a tri-dent complex (Fig. S2†). Therefore, the E_ds for PEI-2 with Li_2S_3 and Li_2S_4 are abnormally high.

To optimize the cross-linking conditions for the preparation of the cathode material, the reaction between PEI and ER was first carried out without sulfur and conductive carbon. Specifically, PEI and ER at different weight ratios (from 2 : 1 to 1 : 5) were dissolved in NMP at a concentration of 20 wt%. It was found that the PEI : ER binder solutions can be stored for 48 h at room temperature without obvious change in viscosity (Fig. S6†), which indicates that these solutions are reasonably stable under ambient conditions. The PEI : ER solutions were blade coated on Al foil substrates and the resulting films were dried briefly in air and then cured in a vacuum oven at 50 °C for 12 h, which are the common conditions for fabricating sulfur cathodes. It was found that when the PEI : ER ratios are in the range between 1 : 1 and 1 : 4, the cross-linked films showed unnoticeable deformation after soaking in the electrolyte solution for 7 days (Fig. S7†), indicating the excellent stability of these films in the electrolyte solution. Next, the PEI–ER resin

with a PEI : ER weight ratio of 1 : 1, 1 : 2, 1 : 3, or 1 : 4 was incorporated as a binder in the cathode material slurry by grinding a mixture of PEI, ER, sublimed sulfur (SS), and a conductive carbon Super P (SP) in NMP to determine the best PEI : ER ratio for optimal battery performance. Commercially available carbon paper (CP) (Toray TGP-H-090), which has a porous 3D structure composed of inter-connected micrometer-sized conductive carbon fibers and sheets (Fig. S8a†), was used as the current collector in this work to avoid cracking of the thick cathode coating with areal sulfur loadings $\geq$2 mg cm^{-2}.[35–37] The SS : SP : PEI–ER weight ratios were maintained at 70 : 20 : 10. The slurries were blade coated on conductive carbon paper (CP) substrates, which were used as the cathode current collectors, and dried and cured in a vacuum oven at 50 °C for 12 h before being assembled into CR2025 coin cells with a configuration that has been mostly adopted for Li–S battery testing (Fig. 2a). It was found that the cathode with a binder PEI–$ER_{1:2}$, which has a PEI : ER weight ratio of 1 : 2, exhibited the optimal overall performance with the highest capacity and the best cycling stability (Fig. S9†). Therefore, a PEI : ER ratio of 1 : 2 was used for further studies.

To gain insight into the reaction between PEI and ER, Fourier-transform infrared spectroscopy (FTIR) was used to characterize the PEI–$ER_{1:2}$ film at different curing times. Specifically, PEI and ER with a weight ratio of 1 : 2 were dissolved in chloroform, coated onto a sodium chloride disc to form a thin film and dried with a nitrogen gas flow. The sample was heated at 50 °C in a vacuum oven prior to the FTIR measurement. As a comparison, the FTIR spectra of pure PEI and ER were also collected. As shown in Fig. 3a, PEI showed the N–H stretching of $–NH_2$ and –NH– groups at 3380 cm^{-1}, $–CH_2$ symmetric and asymmetric stretching at 2954 cm^{-1} and 2839 cm^{-1}, and N–H bending of $–NH_2$ and –NH– groups at 1656 cm^{-1} and 1603 cm^{-1}. ER showed characteristic O–H stretching at 3504 cm^{-1}, $–CH_2–$ stretching of epoxide at 3058 cm^{-1}, C–H stretching of $–CH_2$, $–CH_3$, and aromatic and aliphatic C–H at 2966 cm^{-1}, 2926 cm^{-1} and 2870 cm^{-1}, aromatic –C=C–H stretching at 1606, 1580 and 1509 cm^{-1}, C–O stretching of the aromatic ring at 1184 cm^{-1}, and C–O stretching of epoxide at 916 cm^{-1}.[38–40] As the reaction proceeds, the sample cured for 24 h showed a notable decrease in the intensity of the peak at 916 cm^{-1} representing the C–O stretching of epoxide (Fig. 3a and b). The conversion of epoxide groups (α) was calculated using eqn (1):[41,42]

$$\alpha = 1 - \frac{\frac{A_{916,\,t}}{A_{1184,t}}}{\frac{A_{916,0}}{A_{1184,0}}} \quad (1)$$

where $A_{916,0}$ and $A_{916,t}$ represent the peak areas at 916 cm^{-1} at reaction time zero and t, respectively, and $A_{1184,0}$ and $A_{1184,t}$ represent the peak areas at 1184 cm^{-1} (the C–O stretching of the aromatic ring of ER as an internal reference) at reaction time zero and t, respectively.

As shown in Fig. 3b, the reaction between PEI and ER was quite fast at first with the conversion of epoxide reaching 54% in 2 h and then slowed down likely due to the increased viscosity of the reaction mixture as well as the formation of a cross-linked structure that prevented the movement of the molecules. After curing for 48 h at 50 °C, the conversion of epoxide groups only slightly increased to 66%. Even after the sample was kept under ambient conditions for one week, there were still 28% of unreacted epoxide groups left ($\alpha = 0.72$) in the sample (Fig. 3c).

To evaluate the lithium polysulfide adsorption ability, the PEI–$ER_{1:2}$ binder was soaked in a lithium polysulfide solution and measured by UV-vis spectroscopy. Li_2S_6 was synthesized as an example of lithium polysulfides by reaction between elemental sulfur and Li_2S at a molar ratio of 5 : 1 in a mixed solvent of 1,3-dioxolane (DOL)/1,2-dimethoxyethane (DME) (v/v, 1/1).[30,43] The SP/PEI–$ER_{1:2}$ composite with a carbon/polymer weight ratio of 2 : 1 was added to the Li_2S_6 solution and kept for 24 h before the clear supernatant was taken out for UV-vis absorption measurements. The SP, SP/PVDF composite, SP/PEI composite and SP/ER composite were also tested in a similar manner as comparisons. As shown in Fig. 3d, the blank Li_2S_6 solution showed a yellowish color with a shoulder at ~400 nm in the UV-vis spectrum, which agrees well with the literature.[30,43,44] For the sample mixed with SP, a lighter color and a decrease in the intensity of the shoulder at 400 nm were observed suggesting that SP has some adsorption ability toward Li_2S_6. The sample mixed with SP/PVDF showed a further slight drop in the absorption intensity. In contrast, the samples mixed with SP/PEI, SP/ER and SP/PEI–$ER_{1:2}$ all became colorless and their peak intensities at 400 nm were close to zero indicating that PEI, ER and PEI–$ER_{1:2}$ have much stronger adsorption abilities towards Li_2S_6 than PVDF. The results are in excellent agreement with our theoretical calculations that PEI and ER have much higher binder energies towards lithium polysulfides than PVDF.

Due to the large volume change of sulfur cathodes in Li–S batteries during cycling, the ability of a polymer binder to cushion the mechanical stress inside the battery is important. Next, we evaluated the mechanical properties of our newly developed PEI–ER binders. Cross-linked PEI–ER films were prepared by reaction of pure PEI with ER at different PEI/ER weight ratios from 1 : 1 to 1 : 4 and subjected to a universal tensile test. As shown in Fig. S12,† the tensile strength of the PEI–$ER_{1:1}$ film was only 1.5 MPa, much lower than those of other PEI–ER films, which can be attributed to the low cross-linking density of the PEI–$ER_{1:1}$ film. As the PEI/ER weight ratio increased to 1 : 2, the tensile strength of the resultant film increased from 22.3 MPa. Further increasing the PEI/ER ratio to 1 : 3 and 1 : 4 led to a further increase of the tensile strength to 27.5 and 29.6 MPa, respectively, as a result of increasing cross-linking density. The elongations-at-break of PEI–ER films cross-linked at different PEI/ER weight ratios were similar (10.3–13.8%). The tensile strengths and elongations-at-break of the PEI–ER binders with PEI/ER weight ratios of 1 : 2 to 1 : 4 are similar to those of other polymer binders used for Li–S batteries, *e.g.* carboxymethyl cellulose (CMC) (25.5 MPa and 10.0%)[45] and gelatin (13.5 MPa and 26.5%).[46]

The polymer binder, which takes up 10 wt% of the total cathode in Li–S batteries, is not only responsible for binding sulfur particles, carbon black and the current collector together,

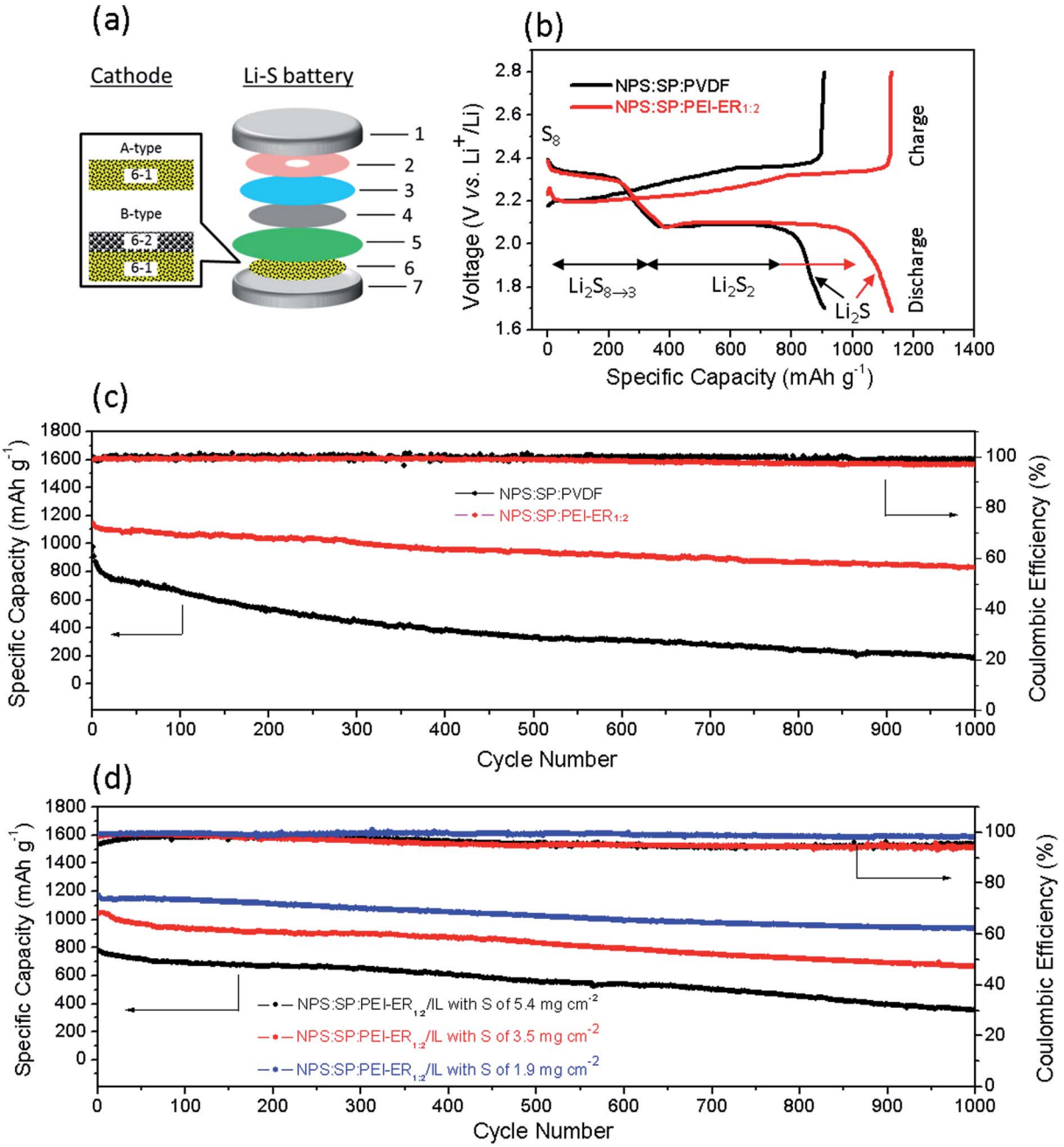

Fig. 2 (a) The configuration of the CR2025 coin button Li–S battery used in this study: (1) anode cover; (2) shrapnel; (3) spacer; (4) Li anode; (5) separator; (6) cathode; (7) cathode cover. Two types of cathode structures were used: Type A is made of a composite layer (6-1), which is comprised of sulphur (sublimed sulphur (SS) or sulphur nanoparticles (NPS)) (70%), conductive carbon black Super P (SP) (20%), and the PEI–EP or PVDF binder (10%), coated on a carbon paper (CP) current collector; Type B is made of a composite layer (6-1) as above and an additional interlayer (IL) (6-2), which is comprised of the conductive component SP (67%) and the PEI–EP binder (33%). (b) Discharge–charge profiles of NPS:SP:PVDF and NPS:SP:PEI–$ER_{1:2}$ cathodes (Type A in (a)) of Li–S batteries at 0.5C. (c). Cycling performance of NPS:SP:PVDF and NPS:SP:PEI–$ER_{1:2}$ cathodes (Type A in (a)) of Li–S batteries at 0.5C. (d). Cycling performance of NPS:SP:PEI–$ER_{1:2}$/IL cathodes (Type B in (a)) with various S loading in Li–S batteries at 0.5C.

but also plays a role in Li^+ ion conduction. A polymer binder with moderate electrolyte solvent uptake and good wettability to the electrolyte solvent is beneficial for Li^+ ion conduction and electrochemical reaction kinetics although excessive absorption of the electrolyte solvent can reduce its binding strength and lead to loss of contact among electrode materials, carbon black and the current collector.[28,47–49] The electrolyte solvent uptake ability can be represented by the swelling ratio, which is defined as the ratio of the mass of the electrolyte solvent absorbed by the polymer film after soaking in the electrolyte solvent to the mass of the polymer film before soaking. As shown in Fig. S13,† PEI–$ER_{1:1}$ showed the highest percent swelling ratio of 26.5%, while

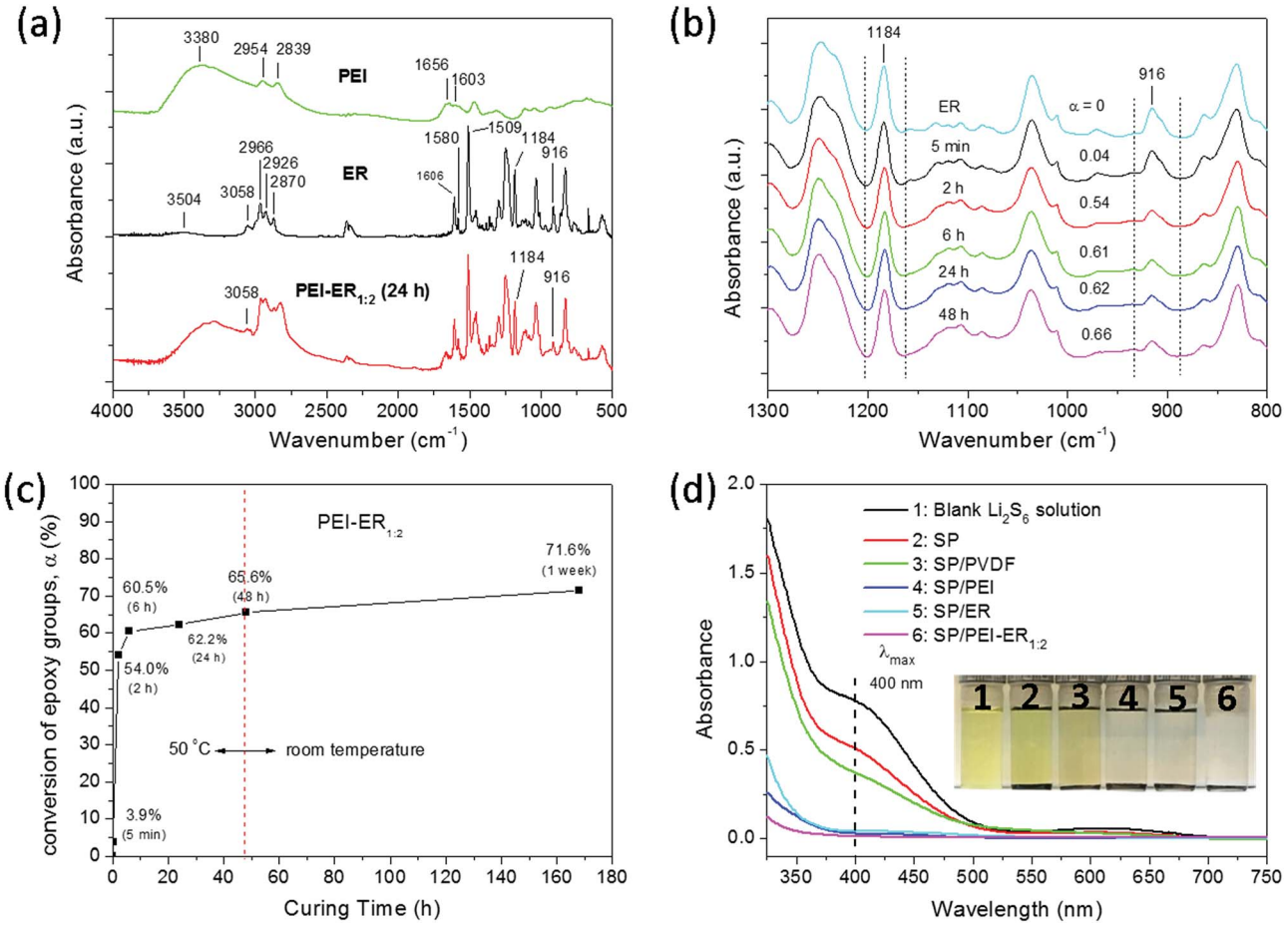

Fig. 3 (a) FT-IR spectra of PEI, ER, and PEI–$ER_{1:2}$ (cured for 24 h at 50 °C under vacuum). (b) FT-IR spectra and the conversion of epoxide groups (α) of pure ER and PEI–$ER_{1:2}$ cured at 50 °C under vacuum for different times. (c) The conversion of epoxide groups (α) of the PEI–$ER_{1:2}$ resin cured at 50 °C for up to 48 hours and kept at room temperature for up to one week. (d) UV-vis absorption spectra of the blank Li_2S_6 solution (0.5 mM) and Li_2S_6 solutions with addition of different absorbents for 24 h at room temperature.

PEI–$ER_{1:3}$ and PEI–$ER_{1:4}$ showed the lowest and similar value of 15.0%. The PEI–$ER_{1:2}$ sample showed a moderate percent swelling ratio of 20.2%. This trend agrees with the increased cross-linking density accompanied with increasing PEI/ER weight ratio, which led to its increased porosity for a higher amount of solvent uptake. The percent swelling ratio of 20.2% for PEI–$ER_{1:2}$ is comparable to other binders in the literature, *e.g.* 20.3% for poly(3,4-ethylenedioxythiophene):poly(styrene-sulfonate) (PEDOT:PSS),[28] 28% for sodium carboxymethyl cellulose (CMC),[49] and 33% for N-guar gum (GG)–xanthan gum (XG).[37] The best stability observed for the battery using the PEI–$ER_{1:2}$ binder (Fig. S9†) is likely due to the balanced mechanical properties and electrolyte uptake ability of this binder.

Next, sublimed sulfur (SS) was replaced with sulfur nanoparticles (NPS) for preparing the cathode material since it was previously reported that a decrease in the sulfur particle size could lead to an enhancement of the cathode capacity.[50] Fig. 2b presents the voltage–capacity profile of a battery using an NPS:SP:PEI–$ER_{1:2}$ cathode during the second cycle. A reference battery using an NPS:SP:PVDF cathode was also fabricated and tested for comparison. The NPS:SP:PVDF cathode exhibits a specific capacity of 908 mA h g^{-1}. The discharge curve shows a typical two-step reduction process involving the formation of lithium polysulfide species (Li_2S_x, x = 3–8) at ~2.3 V, lithium disulfide (Li_2S_2) at ~2.1 V, and lithium sulfide (Li_2S) as the final discharge product.[1,11,51–53] During charging, Li_2S was oxidized to form Li_2S_2 at ~2.2–2.3 V, Li_2S_{3-8} at ~2.3 V and then the final product sulfur at ~2.4 V. The battery with the NPS:SP:PEI–$ER_{1:2}$ cathode showed a significantly increased specific capacity of 1127 mA h g^{-1}. It appears that the first discharge plateau at ~2.2–2.3 V of the NPS:SP:PEI–$ER_{1:2}$ cathode is almost identical to that of the NPS:SP:PVDF cathode, which indicates that the reduction reactions to form the soluble polysulfides (Li_2S_{3-8}) were very similar in these two cathodes. However, the second discharge plateau at ~2.1 V to form Li_2S_2 is much longer for the NPS:SP:PEI–$ER_{1:2}$ cathode, which suggests that a larger amount of the soluble polysulfides were involved in the reduction to form Li_2S_2. The fact that the NPS:SP:PVDF cathode showed an identical first discharge plateau to that of the NPS:SP:PEI–$ER_{1:2}$ cathode might suggest that the diffusion of longer polysulfides (Li_2S_x, where x is >4) in the former seems similar to that of the NPS:SP:PEI–$ER_{1:2}$ cathode probably due to their relatively fast conversion to shorter polysulfides (Li_2S_4 and Li_2S_3). These shorter polysulfides, however, would stay longer (the second

discharge plateau) before being fully reduced to Li_2S_2, which allows them to diffuse away from the conducting network and/or the cathode more readily in the NPS:SP:PVDF cathode. As shown in our DFT simulations, the higher binding energies of PEI–ER, especially the PEI-2 segment, towards Li_2S_3 and Li_2S_4 (Fig. 1b) might be very beneficial for the confinement of these polysulfides, leading to the improved specific capacity of the NPS:SP:PEI–$ER_{1:2}$ cathode.

The long-term cycling performance of NPS:SP:PVDF and NPS:SP:PEI–$ER_{1:2}$ cathodes at a current rate of 0.5C is shown in Fig. 2c and Table 1. The initial discharge specific capacity of the NPS:SP:PVDF cathode is 973 mA h g^{-1}. After 500 charge/discharge cycles, the discharge capacity decreased to 332 mA h g^{-1}, corresponding to a capacity retention of 34% or a decay rate of 0.132% per cycle. The NPS:SP:PEI–$ER_{1:2}$ cathode, however, exhibited a much higher initial capacity of 1145 mA h g^{-1}. After 500 cycles, the cathode still had a capacity of 954 mA h g^{-1} with a capacity retention of 83%. Even after 1000 cycles, the capacity remained at 72% of the initial value. The significant improvement of the cycling stability for the NPS:SP:PEI–$ER_{1:2}$ battery was considered mainly due to the strong binding ability of the cross-linked PEI–ER binder to both sulfur and the soluble lithium sulfides.

To evaluate the binding ability of PEI–ER to elemental sulfur in comparison to PVDF, the NPS:SP:PEI–$ER_{1:2}$ and NPS:SP:PVDF cathode materials were Soxhlet extracted with refluxing CS_2, which is a good solvent for elemental sulfur. The NPS:SP:PEI–$ER_{1:2}$ sample retained 31% of the initially loaded sulfur after extraction for 5 h and still had 26% of sulfur left even after 48 h, whereas the NPS:SP:PVDF sample lost all sulfur within 5 h. The significantly improved solvent resistance of the NPS:SP:PEI–$ER_{1:2}$ sample indicates that the cross-linked PEI–ER binder has a strong ability to retain the elemental sulfur, which would partially contribute to the much improved cycling stability of the NPS:SP:PEI–$ER_{1:2}$ cathode based Li–S battery.

Addition of an appropriate interlayer (IL) between the cathode and the separator has proven to be effective to prevent sulfur loss and migration of soluble polysulfides towards the anode to improve the Li–S battery cycling stability.[54–57] Therefore, a PEI–ER:SP layer with an areal density of 0.17 mg cm^{-2} was added as a protection interlayer on the top surface of the pre-cured NPS:SP:PEI–$ER_{1:2}$ cathode by blade coating a slurry of PEI, ER (with a PEI : ER weight ratio of 1 : 2), and SP with a (PEI + ER) : SP ratio of 1 : 2 and subsequently curing the sample at 50 °C in a vacuum oven for 12 h. The SEM images of the surface of the cathode with this protection layer showed a denser morphology with voids covered by the interlayer in comparison with the cathode without this protection layer (Fig. S8b and c†). The resulting cathode with this interlayer, NPS:SP:PEI–$ER_{1:2}$/IL, exhibited a slightly increased initial specific capacity of 1174 mA h g^{-1} at 0.5C compared with the cathode without the interlayer (Fig. 2 and Table 1). The battery showed a significantly improved cycling stability with a capacity retention of 80% after 1000 cycles, which corresponds to a very low capacity decay rate of 0.02% per cycle. A high coulombic efficiency of >99% was maintained after 1000 cycles. This is among the best cycling stability reported so far for Li–S batteries.[17] These results demonstrated that this additional interlayer could function as an effective barrier to further reduce the loss of sulfur species, leading to this remarkable long-term cycling stability.

The morphology of the sulfur cathode surface before and after cycling (for 1000 cycles) was also studied by SEM. As shown in Fig. S8d,† the NPS:SP:PEI–$ER_{1:2}$ cathode showed micrometer-sized aggregates after cycling, which is likely due to the diffusion (relocation) of the soluble lithium polysulfides and recrystallization of sulfur after charging. The fact that there were no large isolated sulfur crystals formed indicates that the sulfur particles were still well dispersed within the cathode composite together with SP and the PEI–$ER_{1:2}$ binder. On the other hand, the NPS:SP:PEI–ER1:2/IL cathode showed no obvious difference in morphology before and after cycling, indicating that sulfur was mostly confined behind the interlayer.

The above Li–S battery with the NPS:SP:PEI–$ER_{1:2}$/IL cathode has a sulfur loading of 1.9 mg cm^{-2}. The areal capacity is calculated to be 2.2 mA h cm^{-2} (Table 1). To further increase the areal capacity, batteries with higher sulfur loading were fabricated by increasing the amount of the NPS:SP:PEI–$ER_{1:2}$ composite through coating/curing the cathode material slurry two or three times. As shown in Fig. 2d, the cathodes with sulfur

Table 1 Summary of cathode compositions and performance of the corresponding Li–S batteries

Cathode	S loading (mg cm^{-2})	Discharge capacity at 0.5C (mA h g^{-1})		Retention after (n) cycles	Capacity decay rate per cycle	Areal capacity (mA h cm^{-2})
		Initial	After (n) cycles			
NPS:SP:PVDF	1.9	973	332 (500)	34% (500)	0.132% (500)	1.8
			192 (1000)	20% (1000)	0.080% (1000)	
NPS:SP:PEI–$ER_{1:2}$	1.9	1145	940 (500)	83% (500)	0.034%(500)	2.1
			829 (1000)	72% (1000)	0.028% (1000)	
NPS:SP:PEI–$ER_{1:2}$/IL	1.9	1174	1025 (500)	87% (500)	0.026% (500)	2.2
			937 (1000)	80% (1000)	0.020% (1000)	
	3.5	1043	834 (500)	80% (500)	0.040% (500)	3.7
			665 (1000)	64% (1000)	0.036% (1000)	
	5.4	780	558 (500)	72% (500)	0.056% (500)	4.2
			355 (1000)	46% (1000)	0.054% (1000)	

loadings of 3.5 mg cm^{-2} and 5.4 mg cm^{-2} exhibit initial discharge capacities of 1043 mA h g^{-1} and 780 mA h g^{-1} at 0.5C, which correspond to areal capacities of 3.7 mA h cm^{-2} and 4.2 mA h cm^{-2}, respectively. Most Li–S batteries reported in the literature had a sulfur loading lower than 2 mg cm^{-2} and showed specific capacities of less than 1000 mA h g^{-1} or less at 0.5C, which corresponds to areal capacities of less than 2 mA h cm^{-2}.[17] The areal capacity of commercial Li-ion batteries is about 3 mA h cm^{-2}. Therefore, the areal capacity of 4.2 mA h cm^{-2} achieved by our NPS:SP:PEI–$ER_{1:2}$/IL cathode with 5.4 mg cm^{-2} sulfur loading is higher than those of most Li–S batteries reported and the commercial Li-ion batteries. After 500 discharge/charge cycles, the capacities of the batteries with a sulfur loading of 3.5 mg cm^{-2} and 5.4 mg cm^{-2} remained at 833 mA h g^{-1} and 558 mA h g^{-1}, corresponding to a capacity retention of 80% and 72%, respectively. While the cycling stability of these two batteries are still very high, the batteries become less stable with increasing sulfur loading. A similar phenomenon was observed in a previous study of a different type of sulfur cathode for Li–S batteries.[58] One possible reason might be the relatively low electrical conductivity (~5–30 S cm^{-1}) of SP,[59] which resulted in poor charge transport from the sites that are remote from the current collector, resulting in lower sulfur utilization. The use of an alternative conductive component with a higher conductivity may lead to Li–S batteries with a higher areal capacity together with a better cycling stability.

Experimental section

Materials and instrumentation

Polyethylenimine (PEI) (M_w = ~25 000, branched), an epoxy resin compound (ER) (Araldite® 506), polyvinylpyrrolidone (PVP) (M_w = ~40 000), carbon paper (CP) (Toray TGP-H-090), Super P (SP) (Timcal) and other materials were obtained from commercial sources and used as received. FTIR spectra were collected with a Shimadzu 8400S spectrometer. A universal tensile test was carried out on an Instron Series 4400 Universal Testing Instrument with a gauge length of 14.0 mm at a cross-head speed of 0.2 mm min^{-1}. The SEM images of the samples were obtained using a Zeiss LEO 1550 high-resolution field emission scanning electron microscope.

Preparation of PEI, ER and PEI–$ER_{1:2}$ samples for FTIR characterization

PEI in chloroform solution and ER in chloroform solution were prepared. Then a few drops of the solutions were added onto clean NaCl pellets and blow-dried with N_2 gas. Pure PEI and ER with a mass ratio of 1 : 2 were weighed first and immediately diluted with chloroform. A few drops of the PEI–$ER_{1:2}$ solution were added onto a clean NaCl pellet and blow-dried with N_2 gas. After that the pellets were inserted into an FTIR spectrometer for collecting the spectra. For monitoring the cross-linking reaction with FTIR, the same pellet onto which the PEI–$ER_{1:2}$ film was attached was repeatedly put into a 50 °C vacuum oven for reaction and taken out of the vacuum oven for collecting the FTIR spectra at different reaction times (2 h, 6 h, 24 h, and 48 h).

Preparation of PEI–$ER_{1:2}$ films for the tensile test

PEI and ER with weight ratios from 1 : 1 to 1 : 4 were mixed thoroughly in a flask with a glass rod at 0 °C, degassed under vacuum for 5 min, poured into a plastic mold, and transferred into a vacuum oven for a cross-linking reaction at 50 °C for 48 h. The resultant films were cut into strips with dimensions of length 40.0 mm × width 5.0 mm × thickness 0.5 mm for the universal tensile test.

UV-vis absorption measurements

Li_2S_6 was synthesized by reaction of elemental sulfur with Li_2S at a stoichiometric ratio of 5 : 1 in DOL/DME (v/v, 1 : 1) solvent in a sealed vessel at 80 °C overnight. SP/PVDF, SP/PEI, SP/ER and SP/PEI–$ER_{1:2}$ composites were prepared by mixing SP with a polymer at a mass ratio of 2 : 1 in NMP. The slurries were coated onto glass Petri dishes, dried in a convection oven at 50 °C, and then transferred to a vacuum oven at 50 °C. After drying, the resultant solids were ground into fine powders in an agate mortar to eliminate the influence of the particle size. In a typical Li_2S_6 adsorption experiment, 15 mg of Super P/polymer composite which contains 10 mg of Super P and 5 mg of polymer was added into 3.5 mL of 0.5 mM Li_2S_6 solution. The mixture was well mixed by shaking the vial 4 times at an interval of 0.5 h. After being kept at room temperature for 24 h, the clear supernatant was taken out for UV-vis absorption measurements. As a comparison, the Li_2S_6 adsorption of the same amount of Super P (10 mg) was also tested.

Electrolyte solvent uptake test

Pre-weighed cross-linked PEI–ER thin films at PEI/ER weight ratios from 1 : 1 to 1 : 4 with dimensions of length 10.0 mm × width 5.0 mm × thickness 0.5 mm were soaked in mixed DOL/DME solvent (v/v, 1/1) in sealed vials, and taken out for measuring the weight change after certain soaking times. For the PEI–$ER_{1:1}$ and PEI–$ER_{1:2}$ films, the weight change reached the maximum after about 4 days, while it took about one week for PEI–$ER_{1:3}$ and PEI–$ER_{1:4}$ films. After the films were taken out of the electrolyte solvent, they were dried with clean paper towels before weighing. The swelling ratio is defined as the weight of the electrolyte solvent absorbed by the PEI–ER film divided by the weight of the PEI–ER film before soaking.

Synthesis of sulfur nanoparticles (NPS)

Sulfur nanoparticles (NPS) were synthesized following a previously reported method.[60] Aqueous solutions of 80 mM $Na_2S_2O_3$ (50 mL) and 0.4 M PVP (the concentration was based on the repeating unit of PVP) (50 mL) were mixed at room temperature. Then, concentrated hydrochloric acid (0.4 mL; 37%) was added under stirring. After 2 h, the reaction mixture was centrifuged at 4000 rpm for 15 min to isolate the precipitates, which were washed with deionized water 5 times and dried in air and then under vacuum at room temperature. The sulfur content is

~99% as determined by thermogravimetric analysis (TGA) (Fig. S10†). The average diameter of the NPS is ~120 nm estimated by the SEM image (Fig. S11†).

Preparation and solvent resistance testing of cross-linked PEI–ER samples

PEI–ER binders at different PEI : ER weight ratios (2 : 1, 1 : 1, 1 : 2, 1 : 3, 1 : 4, and 1 : 5) were prepared by mixing PEI and ER at a total concentration of 20 wt% in *N*-methyl-2-pyrrolidone (NMP). The solutions were coated on Al foils with a blade. The obtained films were dried briefly in air and then in a vacuum oven at 50 °C for 12 h. To test the solvent resistivity, the PEI–ER films were peeled off from the Al foil and soaked in an electrolyte solution for 7 days. The electrolyte solution used was 1 M lithium bis-trifluoromethanesulfonylimide (LiTFSI) in 1,3-dioxolane (DOL)/dimethoxyethane (DME) (1 : 1, v/v) containing 2 wt% $LiNO_3$. The weight losses of the sample were measured to assess the solvent resistance of sulfur inside the sample (Table S1†).

Preparation of NPS:SP:PEI–ER cathodes

NPS (70 wt%), SP (20 wt%), and a freshly prepared solution of PEI and ER (10 wt%) at different PEI : ER ratios were mixed in NMP with a solid concentration of 20 wt% and the mixture was ground for 40 min in a mortar. The obtained slurry was blade coated on a CP substrate and dried briefly in air and then in a vacuum oven at 50 °C for 12 h. A protective layer comprised of PEI–ER and SP was optionally blade coated on top of the cured NPS:SP:PEI–ER cathode layer and was subjected to cross-linking at 50 °C in a vacuum oven for 12 h. The slurry for coating the protective layer was prepared by mixing PEI and ER (1 : 2) and SP with a total solid content of 20 wt% in NMP, where the (PEI + ER) : SP weight ratio was 1 : 2. The cathode using PVDF as the binder was prepared similarly by blade coating a slurry comprising NPS, SP, and PVDF at weight ratios of 70 : 20 : 10.

Battery assembly and electrochemical measurements

CR2025 coin cells were assembled in an argon-filled glovebox. The battery structure is shown in Fig. 2a. A shrapnel, a spacer, a Li anode film, and a Celgard 2500 separator were placed sequentially in an anode cover. Then the electrolyte (50 μL), 1 M LiTFSI in DOL/DME (1 : 1, v/v) containing 2 wt% $LiNO_3$, was added on top of the separator with a syringe. The CP coated with the cathode material as described above, which was cut into a circular disk with a diameter of 12 mm, was loaded as the cathode. Finally, the stacked layers were pressed to complete the battery assembly. Discharge–charge measurements were carried out within a voltage window of 1.7–2.8 V at different current densities at room temperature on a LAND battery tester.

Conclusions

In summary, we developed an epoxy resin PEI–ER based on a branched polyethylenimine and an epoxy compound for the cathode in Li–S batteries. This epoxy resin formulation can react *in situ* under mild conditions to form a robust cross-linked 3-D network to hold sulfur and the conductive carbon. The abundant nitrogen and oxygen atoms in the PEI–ER binder provide a strong chemical affinity to lithium sulfides, especially the soluble intermediate polysulfides. Moreover, the PEI–ER binder is combined with conductive carbon to form an interlayer between the cathode and the separator to further prevent the shuttling of soluble polysulfides. As a result, the Li–S batteries using the cathode and interlayer made with this binder achieved a high capacity of 1174 mA h g^{-1} and a remarkable cycling performance with a high capacity retention of 80% after 1000 cycles at 0.5C at a sulfur loading of 1.9 mg cm^{-2}. With a high sulfur loading of 5.4 mg cm^{-2}, the battery reached a high areal capacity of 4.2 mA h cm^{-2} and still showed a high capacity retention of up to 72% after 500 cycles at 0.5C. Our study demonstrates that this new polymer binder is very promising for the realization of low cost Li–S batteries with outstanding cycling lifetime and high energy density.

Conflicts of interest

There are no conflicts to declare.

Acknowledgements

This work was supported by the Natural Sciences and Engineering Research Council (NSERC) of Canada (Discovery Grants # RGPIN-2016-04366), the Link Project of the National Natural Science Foundation of China and Guangdong Province (Grant No. U1301244), and the National Natural Science Foundation of China (Grant No. 51573215, 21506260).

References

1 P. G. Bruce, S. A. Freunberger, L. J. Hardwick and J.-M. Tarascon, *Nat. Mater.*, 2011, **11**, 172.
2 Y. Yang, G. Zheng and Y. Cui, *Chem. Soc. Rev.*, 2013, **42**, 3018.
3 S. Evers and L. F. Nazar, *Acc. Chem. Res.*, 2013, **46**, 1135–1143.
4 Y. Zhao, W. Wu, J. Li, Z. Xu and L. Guan, *Adv. Mater.*, 2014, **26**, 5113–5118.
5 Z. Sun, M. Xiao, S. Wang, D. Han, S. Song, G. Chen and Y. Meng, *J. Mater. Chem. A*, 2014, **2**, 9280.
6 X. Li, A. Lushington, Q. Sun, W. Xiao, J. Liu, B. Wang, Y. Ye, K. Nie, Y. Hu, Q. Xiao, R. Li, J. Guo, T.-K. Sham and X. Sun, *Nano Lett.*, 2016, **16**, 3545–3549.
7 Z. Yang, Z. Zhu, J. Ma, D. Xiao, X. Kui, Y. Yao, R. Yu, X. Wei, L. Gu, Y.-S. Hu, H. Li and X. Zhang, *Adv. Energy Mater.*, 2016, **6**, 1600806.
8 M. Yu, J. Ma, H. Song, A. Wang, F. Tian, Y. Wang, H. Qiu and R. Wang, *Energy Environ. Sci.*, 2016, **9**, 1495–1503.
9 Z. Lin, Z. Liu, W. Fu, N. J. Dudney and C. Liang, *Angew. Chem., Int. Ed.*, 2013, **52**, 7460–7463.
10 X.-B. Cheng, J.-Q. Huang, Q. Zhang, H.-J. Peng, M.-Q. Zhao and F. Wei, *Nano Energy*, 2014, **4**, 65–72.
11 R. Fang, S. Zhao, Z. Sun, D.-W. Wang, H.-M. Cheng and F. Li, *Adv. Mater.*, 2017, 1606823.

12 L. Ji, M. Rao, H. Zheng, L. Zhang, Y. Li, W. Duan, J. Guo, E. J. Cairns and Y. Zhang, *J. Am. Chem. Soc.*, 2011, **133**, 18522–18525.
13 X. Ji, K. T. Lee and L. F. Nazar, *Nat. Mater.*, 2009, **8**, 500–506.
14 H. Wang, Y. Yang, Y. Liang, J. T. Robinson, Y. Li, A. Jackson, Y. Cui and H. Dai, *Nano Lett.*, 2011, **11**, 2644–2647.
15 G. Zhou, S. Pei, L. Li, D.-W. Wang, S. Wang, K. Huang, L.-C. Yin, F. Li and H.-M. Cheng, *Adv. Mater.*, 2014, **26**, 625–631.
16 L. Yan, D. Han, M. Xiao, S. Ren, Y. Li, S. Wang and Y. Meng, *J. Mater. Chem. A*, 2017, **5**, 7015–7025.
17 O. Ogoke, G. Wu, X. Wang, A. Casimir, L. Ma, T. Wu and J. Lu, *J. Mater. Chem. A*, 2017, **5**, 448–469.
18 X. Ji, S. Evers, R. Black and L. F. Nazar, *Nat. Commun.*, 2011, **2**, 325.
19 C. Wang, K. Su, W. Wan, H. Guo, H. Zhou, J. Chen, X. Zhang and Y. Huang, *J. Mater. Chem. A*, 2014, **2**, 5018–5023.
20 J. Song, M. L. Gordin, T. Xu, S. Chen, Z. Yu, H. Sohn, J. Lu, Y. Ren, Y. Duan and D. Wang, *Angew. Chem., Int. Ed.*, 2015, **54**, 4325–4329.
21 G. Zhou, Y. Zhao and A. Manthiram, *Adv. Energy Mater.*, 2015, **5**, 1402263.
22 B. D. McCloskey, *J. Phys. Chem. Lett.*, 2015, **6**, 4581–4588.
23 P. D. Frischmann, Y. Hwa, E. J. Cairns and B. A. Helms, *Chem. Mater.*, 2016, **28**, 7414–7421.
24 M. J. Lacey, F. Jeschull, K. Edström and D. Brandell, *J. Power Sources*, 2014, **264**, 8–14.
25 E. Peled, M. Goor, I. Schektman, T. Mukra, Y. Shoval and D. Golodnitsky, *J. Electrochem. Soc.*, 2017, **164**, A5001–A5007.
26 S. S. Zhang, *J. Electrochem. Soc.*, 2012, **159**, A1226–A1229.
27 G. Li, M. Ling, Y. Ye, Z. Li, J. Guo, Y. Yao, J. Zhu, Z. Lin and S. Zhang, *Adv. Energy Mater.*, 2015, **5**, 1500878.
28 J. Pan, G. Xu, B. Ding, Z. Chang, A. Wang, H. Dou and X. Zhang, *RSC Adv.*, 2016, **6**, 40650–40655.
29 P. Bhattacharya, M. I. Nandasiri, D. Lv, A. M. Schwarz, J. T. Darsell, W. A. Henderson, D. A. Tomalia, J. Liu, J.-G. Zhang and J. Xiao, *Nano Energy*, 2016, **19**, 176–186.
30 W. Chen, T. Qian, J. Xiong, N. Xu, X. Liu, J. Liu, J. Zhou, X. Shen, T. Yang, Y. Chen and C. Yan, *Adv. Mater.*, 2017, **29**, 1605160.
31 Y. Jiao, W. Chen, T. Lei, L. Dai, B. Chen, C. Wu and J. Xiong, *Nanoscale Res. Lett.*, 2017, **12**, 195.
32 W. Li, G. Zheng, Y. Yang, Z. W. Seh, N. Liu and Y. Cui, *Proc. Natl. Acad. Sci. U.S.A*, 2013, **110**, 7148–7153.
33 S. S. Zhang, D. T. Tran and Z. Zhang, *J. Mater. Chem. A*, 2014, **2**, 18288–18292.
34 J. H. Kim, J. Seo, J. Choi, D. Shin, M. Carter, Y. Jeon, C. Wang, L. Hu and U. Paik, *ACS Appl. Mater. Interfaces*, 2016, **8**, 20092–20099.
35 H.-J. Peng, J.-Q. Huang, X.-B. Cheng and Q. Zhang, *Adv. Energy Mater.*, 2017, 1700260.
36 Q. Pang, X. Liang, C. Y. Kwok, J. Kulisch and L. F. Nazar, *Adv. Energy Mater.*, 2017, **7**, 1601630.
37 J. Liu, D. G. D. Galpaya, L. Yan, M. Sun, Z. Lin, C. Yan, C. Liang and S. Zhang, *Energy Environ. Sci.*, 2017, **10**, 750–755.
38 L. M. Meng, Y. C. Yuan, M. Z. Rong and M. Q. Zhang, *J. Mater. Chem.*, 2010, **20**, 6030.
39 K. Liu, W. Wu, B. Chen, X. Chen and N. Zhang, *Nanoscale*, 2013, **5**, 5986.
40 F. Wang, P. Liu, T. Nie, H. Wei and Z. Cui, *Int. J. Mol. Sci.*, 2013, **14**, 17–29.
41 G. Nikolic, S. Zlatkovic, M. Cakic, S. Cakic, C. Lacnjevac and Z. Rajic, *Sensors*, 2010, **10**, 684–696.
42 M. G. González, J. C. Cabanelas and J. Baselga, in *Infrared Spectroscopy - Materials Science, Engineering and Technology*, InTech, 2012, vol. 2, pp. 261–284.
43 Z. Sun, J. Zhang, L. Yin, G. Hu, R. Fang, H. M. Cheng and F. Li, *Nat. Commun.*, 2017, **8**, 1–8.
44 A. Kawase, S. Shirai, Y. Yamoto, R. Arakawa and T. Takata, *Phys. Chem. Chem. Phys.*, 2014, **16**, 9344–9350.
45 M. Tabari, *Foods*, 2017, **6**, 41.
46 S. Esteghlal, M. Niakosari, S. M. H. Hosseini, G. R. Mesbahi and G. H. Yousefi, *Int. J. Biol. Macromol.*, 2016, **86**, 242–249.
47 Y. Tsao, Z. Chen, S. Rondeau-Gagné, Q. Zhang, H. Yao, S. Chen, G. Zhou, C. Zu, Y. Cui and Z. Bao, *ACS Energy Lett.*, 2017, **2**, 2454–2462.
48 M. He, L. X. Yuan, W. X. Zhang, X. L. Hu and Y. H. Huang, *J. Phys. Chem. C*, 2011, **115**, 15703–15709.
49 G. Zhou, K. Liu, Y. Fan, M. Yuan, B. Liu, W. Liu, F. Shi, Y. Liu, W. Chen, J. Lopez, D. Zhuo, J. Zhao, Y. Tsao, X. Huang, Q. Zhang and Y. Cui, *ACS Cent. Sci.*, 2018, **4**, 260.
50 H. Chen, C. Wang, W. Dong, W. Lu, Z. Du and L. Chen, *Nano Lett.*, 2015, **15**, 798–802.
51 M. Barghamadi, A. Kapoor and C. Wen, *J. Electrochem. Soc.*, 2013, **160**, A1256–A1263.
52 Z. Lin and C. Liang, *J. Mater. Chem. A*, 2015, **3**, 936–958.
53 D. Zheng, D. Liu, J. B. Harris, T. Ding, J. Si, S. Andrew, D. Qu, X.-Q. Yang and D. Qu, *ACS Appl. Mater. Interfaces*, 2017, **9**, 4326–4332.
54 Y.-S. Su and A. Manthiram, *Nat. Commun.*, 2012, **3**, 1166.
55 A. Manthiram, Y. Fu, S.-H. Chung, C. Zu and Y.-S. Su, *Chem. Rev.*, 2014, **114**, 11751–11787.
56 Z. Xiao, Z. Yang, L. Wang, H. Nie, M. 'e Zhong, Q. Lai, X. Xu, L. Zhang and S. Huang, *Adv. Mater.*, 2015, **27**, 2891–2898.
57 J.-G. Wang, K. Xie and B. Wei, *Nano Energy*, 2015, **15**, 413–444.
58 N. He, L. Zhong, M. Xiao, S. Wang, D. Han and Y. Meng, *Sci. Rep.*, 2016, **6**, 33871.
59 V. Palomares, A. Goñi, I. G. de Muro, I. de Meatza, M. Bengoechea, I. Cantero and T. Rojo, *J. Power Sources*, 2010, **195**, 7661–7668.
60 Z. W. Seh, Q. Zhang, W. Li, G. Zheng, H. Yao and Y. Cui, *Chem. Sci.*, 2013, **4**, 3673.